JOURNAL OF GEOPHYSICAL RESEARCH, VOL. 101, NO. C2, PAGES 3697–3713, FEBRUARY 15, 1996

Observations and simulations of physical and biological processes at ocean weather station P, 1951–1980

Charles R. McClain and Kevin Arrigo
Oceans and Ice Branch, NASA Goddard Space Flight Center, Greenbelt, Maryland

King-Sheng Tai
General Sciences Corporation, Laurel, Maryland

Daniella Turk
Department of Oceanography, Dalhousie University, Halifax, Nova Scotia, Canada

Abstract. Physical and biological processes in the mixed layer at ocean weather station (OWS) P (50°N, 145°W) over a 30-year period (1951–1980) were investigated using observations and model simulations. The observations include 30 years of surface meteorological and sea surface temperature data collected at OWS P and Ekman upwelling velocities derived from the Comprehensive Ocean-Atmosphere Data Set, 14 years (1953–1966) of daily temperature profiles, nearly 150 chlorophyll *a* profiles spanning all months of the year, monthly climatological solar irradiances, and 0- to 50-m integrated nitrate concentrations. The simulations incorporated models for the estimation of surface solar downwelling irradiance, surface heat fluxes, subsurface diffuse attenuation, mixed layer dynamics, and biological processes. The time-dependent model inputs were the surface observations of cloud cover, air temperature, dew point temperature, and wind speed. The atmospheric irradiance, marine diffuse attenuation, and mixed layer models were adapted from existing models developed by others. The biological model, developed by the authors, has four components (nitrate, ammonium, phytoplankton nitrogen, and zooplankton nitrogen) and computes a variety of additional quantities including chlorophyll *a* concentration and gross and new production. Model comparisons with in situ time series showed that predictions of sea surface temperature and mixed layer depth were reasonably accurate. Climatological monthly profiles of chlorophyll *a* and temperature were within 1 standard deviation of the observed values at nearly all depths. Also, the climatological annual cycles of solar irradiance and 0- to 50-m integrated nitrate accurately reproduced observed values. Annual primary production was estimated to be $\sim$190 g C m^{-2} yr^{-1} and varied by no more than $\pm$5% in any year. This estimate is consistent with recent observations but is much greater than earlier estimates, indicating that carbon cycling in the North Pacific is much more important to the global carbon budget than previously thought. Significant interannual variability in sea surface temperature, Ekman upwelling, mixed layer depth, and surface nitrate concentration had little impact on productivity. The model also indicates that the nitrate supply to the euphotic zone is very sensitive to Ekman upwelling and that amplification of the wind stress curl can result in complete nitrate depletion when the winds are persistently downwelling favorable.

1. Introduction

Recent concern about increased levels of atmospheric CO_2 and global warming have led to studies of the ocean's role in the global carbon budget, e.g., the Joint Global Ocean Flux Study (JGOFS), and increased interest in interannual and interdecadal oceanic variability [*Ocean Studies Board*, 1994; *Subcommittee on Global Change Research*, 1995]. Examination of historical data for these purposes is difficult because of the paucity of comprehensive time series data of sufficient accuracy and duration. For meteorological and hydrographic data the ocean weather stations (OWS) and the Comprehensive Ocean-Atmosphere Data Set (COADS) [*Woodruff et al.*, 1987] provide high-quality meteorological observations, and at some OWS sites, hydrographic time series are available. However, long time series of biological quantities, e.g., profiles of chlorophyll *a* (chl *a*) and column-integrated primary productivity, are relatively scarce, and only recently have comprehensive time series been initiated at Hawaii [*Chriswell et al.*, 1990] and Bermuda [*Knap et al.*, 1991]. Alternatively, investigations of the impact of long-term changes in meteorological forcing on ocean physics and biology can be pursued using coupled models of physical and biological processes. Examples of short-duration ecosystem modeling studies include *Janowitz and Kamykowski* [1991] and *Marra and Ho* [1993].

Inferences about interannual biological variability in the

Paper number 95JC03052.
0148-0227/96/95JC-03052$05.00

North Pacific have been made by *Emerson* [1987] at OWS P (50°N, 145°W) and by *Venrick et al.* [1987] near 29°N, 154°W. Emerson estimated that new production between May and August during 1969–1978 varied annually from 100 to 300 mg C m^{-2} d^{-1}. Venrick et al. reported a sudden increase in integrated chl *a* concentrations during the early 1970s in association with anomalies in sea level pressure and SST. However, *Falkowski and Wilson* [1992] have questioned this observation based on historical Secchi depth data which suggest that chl *a* concentrations have changed little over the past 70 years. If the long-term change in phytoplankton standing crop is significant, it is not known whether this change is a consequence of local or remote forcing and what variables controlling chl *a* concentrations are being affected.

Glover et al. [1994] demonstrated that the pigment transition zone extending across the Pacific basin at middle latitudes, which separates regions of relatively low and high pigment concentrations, coincides with the transition from relatively shallow to deep mixed layer depth (MLD) and low to high nitrate concentrations. Despite the significant annual fluctuation in MLD and temperature north of the transition zone, phytoplankton biomass remains relatively stable throughout the annual cycle [*Clemons and Miller*, 1984; *Venrick*, 1993] and is in dramatic contrast to the North Atlantic [*Evans and Parslow*, 1985] which experiences a pronounced spring bloom preceded by deep wintertime mixed layers (much deeper than in the North Pacific). *Frost* [1987, 1991, 1993] modeled the annual cycle of biological processes in the North Pacific and concluded that zooplankton grazing is the most probable cause of the stable phytoplankton concentrations but allowed that trace nutrients such as iron may play a role. Previous mixed layer and biological studies of the North Pacific (e.g., Subarctic Pacific Ecosystem Research (SUPER); see special issue of *Progress in Oceanography*, *32*, 1993) demonstrate that physical and biological processes can be simulated and that there is feedback between them. However, none of these models is fully prognostic and therefore requires specification of the physical or biological quantities not modeled. For example, the most comprehensive ecological model of the subarctic Pacific to date is by *Frost* [1993]. However, *Frost* [1993] did not explicitly model physical variables but, rather, relied on observations of mixed layer depth, mixed layer temperature, and mean daily solar irradiance for a single year (1970).

OWS P is ideal for studying the effects of meteorological forcing [*Denman and Miyake*, 1973; *Large et al.*, 1994] because it is subject to a large seasonal temperature (heat flux) cycle and is horizontally uniform with minimal horizontal advection. The climatological Ekman upwelling is positive but small because OWS P is located near the climatological transition between positive and negative wind stress curl [*Reinecker and Ehret*, 1988]. Thus most of the vertical fluxes of heat and nutrients are driven by mechanical mixing and buoyancy effects. One important conclusion of *Martin* [1985] was that knowledge of the optical properties which control the vertical distribution of light absorption is key to understanding the behavior of the mixed layer and in estimating the performance of mixed layer models. For OWS P the optical properties are controlled by biological processes and are classified by *Mueller and Lang* [1989].

The objectives of this study were to (1) examine the couplings between local physical and biological processes, (2) examine seasonal and interannual variability in the physics and biology, and (3) evaluate the magnitude of annual primary production at OWS P. The approach was to develop a time-dependent coupled model which explicitly incorporates the interdependencies among the hydrographic, biological, and optical variables and utilizes the observed surface meteorological time series for calculating the surface forcing (mechanical and radiative). Model performance was evaluated using hydrographic time series and historical biological observations.

2. Model Description

The ocean model incorporates a one-dimensional dynamical mixed layer model [*Garwood*, 1977; *Martin*, 1985], a four-component nitrogen-based biological (phytoplankton-zooplankton-nitrate-ammonium) model, and a simple optical model. Surface solar irradiance is computed using the model of *Frouin et al.* [1989] corrected for cloud cover. The structure of the combined model is shown in Figure 1a. The mixed layer and biological components are coupled through the modulation of light and temperature due to absorption of solar radiation by phytoplankton and the temporal and vertical variation in eddy diffusivity as scaled to the surface wind stress and MLD, respectively. The absorbed heat contributes to the overall energy balance which also includes the three surface heat fluxes (latent, sensible, and long wave radiation). The feedback to the biology is completed through the dependency of phytoplankton growth on temperature and the specification of time- and depth-dependent eddy diffusivity.

As discussed by *Lewis et al.* [1984], the space scales (meters to tens of meters) and timescales (hours to days) of vertical

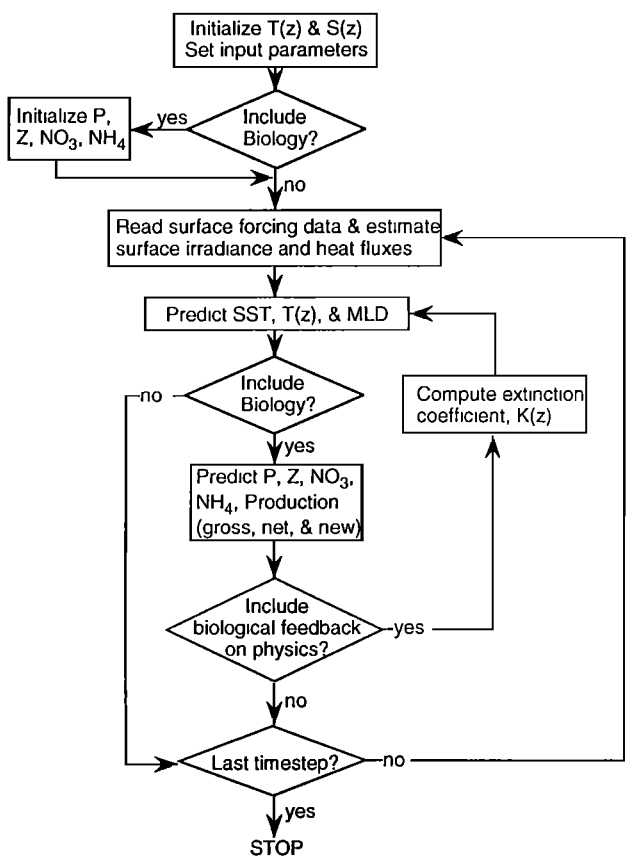

Figure 1a. Flow diagram for the coupled physical-biological model.

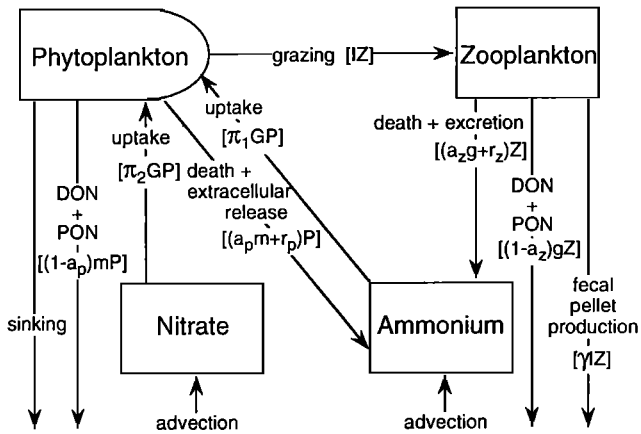

Figure 1b. Flow diagram for the biological model.

phytoplankton variability are determined by the MLD, the diffuse attenuation coefficient, the eddy diffusivity, and the rate of photoadaptation. With these considerations in mind, the model was executed at 1-m vertical and 1-hour temporal resolution. This resolution is sufficiently fine compared with the inherent space scales and timescales to allow the use of coupled physical and biological models rather than a model which integrates the physical and biological dynamics into a single formulation. This strategy allows the development effort to focus on the biological model where the most uncertainty resides and also provides the flexibility to link the biological model to any number of currently available mixed layer models [e.g., *Chen et al.*, 1994] or to improved models in the future.

The model is driven by time-dependent surface illumination and atmospheric forcing fields which must be specified, along with the initial profiles of the primary hydrographic quantities (temperature and salinity) and the four principal biological variables (phytoplankton nitrogen, zooplankton nitrogen, ammonium, and nitrate). The model is allowed to run for 30 years (1951–1980) without reinitialization of any variables. Figure 1b shows the linkages within the biological model. These connections will be described in detail below.

2.1. Solar Irradiance Model

Frouin et al. [1989] estimate the downwelling clear sky solar irradiance E_{clear} for two spectral domains, 350–700 nm (photosynthetically available radiation (PAR)) and 250–4000 nm. PAR rather than spectral irradiance is used to drive phytoplankton growth. This is a reasonable approach in low biomass case 1 [*Morel and Prieur*, 1977] waters where only one phytoplankton species of constant specific absorption is assumed. In fact, simulations using a fully spectral version of the coupled model produced nearly identical monthly climatological chlorophyll *a* and temperature profiles to the present model, but at significant computational expense.

The near-infrared irradiance is calculated using the approximation

$$E_{\text{clear}}(700\text{–}4000) \approx E_{\text{clear}}(250\text{–}4000) - E_{\text{clear}}(350\text{–}700) \tag{1}$$

The error introduced by including the irradiance between 250 and 350 nm is small.

The model inputs include ozone concentration, aerosol type (marine or continental), and visibility. A constant ozone concentration of 340 Dobson units is used, and the aerosol type is assumed to be marine. Visibility (V) is computed at each time step from the relative humidity (for the range of 65 to 99%) using the equation [*Neuberger*, 1951]:

$$\mathrm{V} = 231 - 2.3\mathrm{RH} \tag{2}$$

where RH is the relative humidity (in percent). For RH < 65%, V = 80 km. RH is determined using

$$\mathrm{RH} = \frac{e_{dp}(\mathrm{T})}{e_a(\mathrm{T})}\,100 \tag{3}$$

where e_a is the vapor pressure at the observed temperature and e_{dp} is the vapor pressure at the observed dew point temperature [*Smith*, 1966]. Vapor pressure is related to temperature by

$$e(\mathrm{T}) = a_0 \exp\left(\frac{a_1\mathrm{T}}{a_2 + \mathrm{T}}\right) \tag{4}$$

where $a_0 = 6.1078$, $a_1 = 17.269$, $a_2 = 237.29°$, and T is the temperature (degrees Celsius) of either air or water [*Tetens*, 1930].

Clear sky irradiance is modified to account for the observed cloud cover by applying a power law correction tuned to yield the observed climatological monthly mean surface irradiances [*Dobson and Smith*, 1988],

$$E_{\text{surf}} = E_{\text{clear}}(1 - 0.53c^{0.5}) \tag{5}$$

where E_{surf} is the downwelling surface irradiance and c is fractional cloud cover.

The irradiance that penetrates the ocean surface, $E(0)$, is computed as

$$E(0) = (1 - \mu)E_{\text{surf}} \tag{6}$$

where μ is the surface reflectivity. The surface reflectivity consists of three components,

$$\mu = \mu_d + \mu_f + \mu_{ss} \tag{7}$$

where μ_d is the direct specular reflectance, μ_f is the reflectance from foam, and μ_{ss} is the subsurface reflectance due to molecular and particulate backscatter. The direct reflectance is taken to be the Fresnel reflectance for a flat surface unless the solar zenith angle >40° and the wind speed W is greater than 2 m s^{-1}. If these two conditions are satisfied [*Austin*, 1974],

$$\mu_d = 0.0253 \exp[b(\theta_o - 40)] \tag{8}$$

where θ_o is the solar zenith angle and

$$b = -0.000714W + 0.0618 \tag{9}$$

The foam reflectance is computed as the product of the effective reflectance of foam (0.22 [*Koepke*, 1984]) and the wind-speed-dependent fraction of the surface covered by foam [*Monahan and O'Muircheartaigh*, 1980] or

$$\mu_f = 6.49 \times 10^{-7} W^{3.52} \tag{10}$$

For chl *a* concentrations <2 mg m^{-3} in case 1 water, μ_{ss} is approximately 0.04 [*Morel*, 1988].

After obtaining $E(0)$, the downwelling irradiance at depth z (the vertical coordinate decreases in the downward direction) is estimated by

$$E(z) = E(z - \Delta z) \exp[-K(z)\Delta z] \quad (11)$$

where K is the downwelling diffuse attenuation coefficient. In this analysis the K associated with each wavelength domain, PAR and the near-infrared, is determined independently. K(PAR) is computed as a function of the chl *a* concentration at each depth (*Morel* [1988]; see also *Wroblewski and Richman* [1987] and *Frost* [1993]):

$$K(z, \text{PAR}) = K_w(\text{PAR}) + 0.0518\ \text{chl}(z)^{0.428} \quad (12)$$

where K_w (PAR) is the effective clear water diffuse attenuation coefficient (0.027 m^{-1}) and chl(z) is the chl *a* concentration at depth z. It should be noted that the monthly mean profiles of PAR obtained from this formulation were not substantially different from those obtained when integrating the spectral version of the model from 400 to 700 nm. For the near-infrared, K(NIR) is the effective value of K_w (NIR) over the wavelength band of 700–4000 nm and is assumed to be a constant ≈2.5 m^{-1} [*Baker and Smith*, 1982]. The two wavelength bands are handled separately in the heat absorption calculation. The near-infrared radiation is essentially captured within the first meter of the water column.

The rate of heating at a given depth due to the absorption of downwelling irradiance is given by

$$\frac{dT(z)}{dt} = \frac{[E(z - \Delta z, \text{PAR}) - E(z, \text{PAR}) + E(z - \Delta z, \text{NIR}) - E(z, \text{NIR})]\Delta z}{\rho_w c_{pw}} \quad (13)$$

where ρ_w and c_{pw} are the density and heat capacity, respectively, of water.

2.2. Mixed Layer Model

The MLD is calculated using an updated version of the *Garwood* [1977] one-dimensional (1-D) dynamical mixed layer model. This model predicts the rate of deepening or retreat of the mixed layer as a result of entrainment and detrainment processes at its lower boundary. Aside from the modifications required to implement the irradiance model described above, several minor modifications to the mixed layer model have been made including (1) the use of the wind drag coefficient formulation of *Large and Pond* [1982]; (2) the implementation of the long wave radiation formulation of *Berliand and Berliand* [1952]; (3) the application of simulated rather than observed sea surface temperatures (SSTs) for surface heat flux calculations; (4) the estimation of the MLD using a *Levitus* [1982] temperature difference criterion, T(0) − T(z) = 0.1°, the value suggested by *Martin* [1985] for OWS P; (5) the incorporation of an Ekman vertical velocity term in the MLD computation; and (6) a minimum MLD of 30 m (required to obtain realistic summer temperature profiles).

The input surface meteorological forcing includes both horizontal wind components, surface air temperature, dew point temperature, cloud cover, and visibility. On the basis of these inputs and the chl *a* profile from the previous time step, the model estimates the absorption of short wave radiation and latent, sensible, and long wave radiation surface heat fluxes to determine the mixed layer temperature.

The wind stress is computed from the wind vector W using the standard bulk formula and the drag coefficient formulation of *Large and Pond* [1982]:

$$\tau_{u,v} = \rho_a C_d W_{u,v} |W| \quad (14)$$

where

$$C_d = \left(\frac{2.7}{W} + 0.142 + 0.0764 \left| W \right| \right) 10^{-3} \quad (15)$$

and $\tau_{u,v}$ are zonal and meridional wind stresses, $W_{u,v}$ are zonal and meridional wind components, $|W|$ is the wind speed (meters per second), C_d is the drag coefficient, and ρ_a is the density of air.

The long wave infrared radiation Q_b emitted from the surface is estimated using the formulation of *Berliand and Berliand* [1952]

$$Q_b = \varepsilon\sigma T_a^4(0.39 - 0.58e_a^{0.5})(1 - \alpha c^2) + 4\varepsilon\sigma T_a^3(\text{SST} - T_a) \quad (16)$$

where ε is the emissivity of seawater (0.97), σ is Stefan-Boltzmann constant, T_a is air temperature, e_a is the vapor pressure of air, c is the fractional cloud cover (same as in (5)), and α is a latitude-dependent cloud type parameter which *Berliand and Berliand* [1952] estimated to be 0.72 for 50°N (see *Budyko* [1974] for a complete discussion of this equation).

The calculations of sensible Q_s and latent heat Q_l use the bulk formulas:

$$Q_s = c_s c_{pa} \rho_a |W| (\text{SST} - T_a) \quad (17)$$

$$Q_l = 6.21 \times 10^{-4} c_l l_e \rho_a |W| (0.98 e_w - e_a) \quad (18)$$

where c_s and c_l are the transfer coefficients for sensible and latent heat fluxes, respectively (0.00149 [*Martin*, 1985]); c_{pa} is the specific heat capacity of air (1.0 J g^{-1} °C^{-1}); l_e is the latent heat of vaporization (2488 J g^{-1}); and e_w and e_a are surface vapor pressures (millibars) for water and air, respectively.

As mentioned above, the model allows for Ekman pumping at the base of the mixed layer. The Ekman upwelling w_e is computed from the horizontal wind field using *McClain and Firestone* [1993]

$$w_e(D_e) = \frac{\text{curl}_z(\tau/f)}{\rho_w} \quad (19)$$

where f is the Coriolis parameter, curl_z is a vector operator defined as $(\partial/\partial x - \partial/\partial y)$, and D_e is the Ekman layer depth. Using *Pond and Pickard* [1978], the Ekman layer depth varies as a function of $|W|$ and latitude ϕ such that

$$D_e = \frac{3091 C_d |W|}{[\sin(|\phi|)]^{0.5}} \quad (20)$$

Because w_e is computed from monthly mean gridded wind fields, the values may be underestimated. Therefore the w_e time series can be amplified by a multiplicative constant in the model.

Ekman upwelling varies with depth according to

$$w_e(z) = w_e(D_e) R(z) \quad (21)$$

where $w_e(D_e)$ is the Ekman upwelling at depth D_e and R is the ratio of the Ekman upwelling velocity at depth z to the velocity at the base of the Ekman layer D_e. For simplicity, R is calculated using a canonical profile derived from Ekman theory using the assumptions that $\tau_x = \partial\tau_y/\partial y = \partial\tau_x/\partial y = 0$, resulting in

Table 1. Ecological Model Input Parameter Definitions and Values

Symbol	This Study	Reference 1	Reference 2	Reference 3	Definition
			Initial Conditions		
P	0.2	···	···	···	phytoplankton, mg-at N m^{-3}
Z	0.1	···	···	···	zooplankton, mg-at N m^{-3}
NO_3	depth dependent	···	···	···	nitrate, mg-at N m^{-3}
NH_4	0.1	···	···	···	ammonium, mg-at N m^{-3}
			Phytoplankton Parameters		
m	0	0	0.1	0.045	death rate, d^{-1}
G_0	0.851	0.851	···	···	growth rate at 0°C, d^{-1}
k_{gp}	0.0633	···	···	···	temperature sensitivity of algal growth, $°C^{-1}$
r_{p0}	0.02	···	···	···	respiration rate at 0°C, d^{-1}
k_{rp}	0.0633	···	···	···	temperature sensitivity of algal respiration, $°C^{-1}$
$I_{k\max}$(<60 m)	25	···	···	···	maximum photoacclimation parameter, μEin m^{-2} s^{-1}
$I_{k\max}$(≥60 m)	250	···	···	···	maximum photoacclimation parameter, μEin m^{-2} s^{-1}
K_{NO3}	1.0	···	0.2	0.5	half saturation for nitrate uptake, mg-at N m^{-3}
K_{NH4}	0.1	0.1	···	0.5	half saturation for NH_4 uptake, mg-at N m^{-3}
pk	3	···	1.5	1.5	ammonium inhibition of NO_3 uptake, dimensionless
$S_{\max}$	1.0	···	···	1.0	maximum sinking rate, m d^{-1}
chl a:N	1.0	1.32	···	···	chlorophyll a:nitrogen ratio, mg:mg atm
			Zooplankton Parameters		
g	0.04	···	0.1	0.05	death rate, d^{-1}
R_m	~1.6	1–1.7	1.0	1.0	maximum grazing rate, d^{-1}
Λ	0.8	···	0.75	···	Ivlev constant, m^3 mg-at N^{-1}
	0.0	10.0	···	0.0	minimum C threshold for grazing, mg C m^{-3}
γ	0.3	0.3	0.3	···	unassimilated ingested ration, dimensionless
r_{zo}	0.019	···	···	···	respiration rate at 0°C, d^{-1}
k_{rz}	0.15	···	···	···	temperature sensitivity of respiration, $°C^{-1}$
			Nutrient Parameters		
a_z	0.5	0.4	···	0.33	fraction of dead zooplankton converted to NH_4
a_p	0.5	0.4	···	···	fraction of dead phytoplankton converted to NH_4

References are 1, *Frost* [1993]; 2, *Glover et al.* [1994]; and 3, *Fasham et al.* [1990].

$$R(z) = 0.96\left[1 - \cos\left(\frac{\pi}{D_e}z\right)\exp\left(\frac{-\pi}{D_e}z\right)\right] \quad (22)$$

such that $R(z)$ varies from 0 at the surface to 1 at $z = D_e$.

At each time step the rate of change in the MLD as computed by the *Garwood* [1977] model is augmented by the vertical Ekman velocity calculated at the base of the mixed layer, i.e.,

$$\mathrm{MLD} = \mathrm{MLD_G} + w_e\Delta t \quad (23)$$

where $\mathrm{MLD_G}$ (negative value) is the mixed layer depth computed by the Garwood model.

2.3. Biological Processes

The following system of coupled differential equations simulates the dynamics of phytoplankton nitrogen (P), microzooplankton nitrogen (Z), ammonium (NH_4), and nitrate (NO_3) stocks within the upper ocean:

$$\frac{\partial \mathrm{P}}{\partial t} + w_e\frac{\partial \mathrm{P}}{\partial z} + \frac{\partial \mathrm{SP}}{\partial z} - \frac{\partial}{\partial z}\left(K_v\frac{\partial \mathrm{P}}{\partial z}\right) = \mathrm{GP} - m\mathrm{P} - r_p\mathrm{P} - I\mathrm{Z} \quad (24a)$$

$$\frac{\partial \mathrm{Z}}{\partial t} + w_e\frac{\partial \mathrm{Z}}{\partial z} - \frac{\partial}{\partial z}\left(K_v\frac{\partial \mathrm{Z}}{\partial z}\right) = (1-\gamma)I\mathrm{Z} - g\mathrm{Z} - r_z\mathrm{Z} \quad (24b)$$

$$\frac{\partial \mathrm{NH_4}}{\partial t} + w_e\frac{\partial \mathrm{NH_4}}{\partial z} - \frac{\partial}{\partial z}\left(K_v\frac{\partial \mathrm{NH_4}}{\partial z}\right) = -\pi_1\mathrm{GP} + a_p m\mathrm{P} + r_p\mathrm{P} + a_z g\mathrm{Z} + r_z\mathrm{Z} \quad (24c)$$

$$\frac{\partial \mathrm{NO_3}}{\partial t} + w_e\frac{\partial \mathrm{NO_3}}{\partial z} - \frac{\partial}{\partial z}\left(K_v\frac{\partial \mathrm{NO_3}}{\partial z}\right) = -\pi_2\mathrm{GP} \quad (24d)$$

Definitions and units are defined in the following sections and in Table 1. The coordinate system origin is at the surface and negative downward. To prevent numerical instability when solving (24a)–(24d), the Crank-Nicholson scheme [*Press et al.*, 1988] has been applied. This involves the simultaneous solution of these linear equations for each time step and each depth using the method of Gaussian elimination for tridiagonal systems. The Neumann boundary condition, $\partial X/\partial z = 0$, is applied at both the surface and lower (350 m) model domain boundaries for P and Z. Initial profiles of temperature and NO_3 were obtained from winter and annual climatologies, respectively. Depth-independent initial concentrations of P, Z, and NH_4 are given in Table 1. For NH_4 and NO_3 a fixed value equal to the initial condition was applied at the lower boundary and the Neumann condition was applied at the surface.

The time- and depth-dependent formulation for eddy diffusivity K_v at the surface follows *Csanady* [1982] and was also used by *Janowitz and Kamykowski* [1991], i.e.,

$$K_v(0) = \left|\frac{\tau}{200\rho_w f}\right| \quad (25)$$

K_v is assumed constant throughout the mixed layer but is smoothly decreased to a fraction of $K_v(0)$ within a transition layer just below the mixed layer. The transition layer depth (25 m) and $K_v(0)$ fraction (0.035) were determined by comparing

observed and simulated nitrate profiles and 0- to 50-m integrated nitrate values so as to yield the best results. Below the transition layer, K_v is linearly reduced to a value of 2×10^{-6} m^2 s^{-1} at the lower model boundary.

The rate of phytoplankton sinking (meters per day) accelerates as nutrients are depleted according to [*Eslinger and Iverson*, 1996]:

$$S = S_{max}[1 - \tanh (S_k\ NO_3)] \tag{26}$$

where

$$S_k = 2.16K_N \tag{27}$$

and S_{max} is the maximum sinking rate (meters per day) below the euphotic zone or when nutrients are exhausted. K_N is the nitrate concentration at which phytoplankton growth is half of its maximum rate and the constant 2.16 is in units of (mg-at $m^{-3})^{-2}$, where mg-at is milligram-atoms.

The rate of phytoplankton growth G is calculated as the product of the maximum temperature-dependent growth rate G_m and a dimensionless resource limitation coefficient β such that

$$G = \beta G_m \tag{28}$$

where G and G_m have units of d^{-1}. G_m is a first-order exponential function of temperature [*Eppley*, 1972]:

$$G_m = G_0 \exp (k_{gp}T) \tag{29}$$

where G_0 (d^{-1}) is the specific growth rate at 0°C and k_{gp} ($°C^{-1}$) is a rate constant which determines the sensitivity of G_m to changes in T. Eppley determined G_0 and k_{gp} to be 0.8511 and 0.0633, respectively, based on the growth of a variety of phytoplankton species acclimated to temperatures above 2°C.

β is the resource limitation term calculated as the smaller of the computed nutrient and light limitation terms (N_{lim} and L_{lim}, respectively), i.e.,

$$\beta = \min (N_{lim}, L_{lim}) \tag{30}$$

Nitrogen is assumed to be the nutrient most responsible for controlling algal growth so NO_3 and NH_4 are the only nutrients included in the model. The nitrogen source least limiting to algal growth will be used to estimate β. NH_{4lim} is calculated using the equation of *Monod* [1942],

$$NH_{4lim} = \frac{NH_4}{K_{NH4} + NH_4} \tag{31}$$

where K_{NH4} is the NH_4 concentration where growth is half-maximal. NO_{3lim} is calculated in a similar manner, but with the addition of a term to correct for inhibition of NO_3 uptake due to the presence of NH_4 [*Wroblewski*, 1977],

$$NO_{3lim} = \frac{NO_3}{K_{NO3} + NO_3} \exp (-pk\ NH_4) \tag{32}$$

where K_{NO3} is the NO_3 concentration where growth is half-maximal and pk determines the sensitivity of NO_3 uptake to the presence of NH_4. Finally,

$$N_{lim} = \max (NH_{4lim}, NO_{3lim}). \tag{33}$$

Similarly, the dimensionless light limitation term L_{lim} is given by *Arrigo and Sullivan* [1994]:

$$L_{lim} = 1 - \exp \left(-\frac{E}{I_k} \right) \tag{34}$$

where E is the ambient irradiance ($\mu E\ m^{-2}\ s^{-1}$, with E being einsteins) and I_k is the photoadaptation parameter ($\mu E\ m^{-2}\ s^{-1}$). It has been shown that the photosynthetic characteristics of phytoplankton vary as a function of light history [*Steeman-Nielsen et al.*, 1962; *Kremer and Nixon*, 1978; *Lizotte and Arrigo*, 1994]. Therefore depth-dependent changes in I_k are computed as

$$I_k = \frac{I_{kmax}}{1 + 10 \exp (-BE^*)} \tag{35}$$

where I_{kmax} is the maximum photoadaptation parameter, E^* is the 1-day moving average irradiance, and B is given by

$$B = \exp [1.089 - 2.12 \log (I_{kmax})] \tag{36}$$

With B defined in this way, I_k approaches asymptotic minimum and maximum values at low and high irradiances, respectively, and is approximately equal to E^* at intermediate light levels.

Total N demand must be partitioned into NH_4 and NO_3 uptake defined by the fractions π_1 and π_2, respectively, where

$$\pi_1 = \frac{NH_{4lim}}{NH_{4lim} + NO_{3lim}} \tag{37a}$$

$$\pi_2 = \frac{NO_{3lim}}{NH_{4lim} + NO_{3lim}} \tag{37b}$$

and $\pi_1 + \pi_2 = 1$. Calculation of π_1 and π_2 allows total gross production (GP) to be partitioned into new and regenerated production [*Dugdale and Goering*, 1967], i.e.,

$$\text{new production} = \pi_2\ GP \tag{38}$$

$$\text{regenerated production} = \pi_1\ GP, \tag{39}$$

respectively. The f ratio is the proportion of nitrogen-based growth satisfied by NO_3 [*Eppley and Peterson*, 1979] and is equivalent to π_2.

Zooplankton growth, $(1 - \gamma)IZ$, is determined by the assimilation efficiency, $(1 - \gamma)$, and the herbivore grazing term [*Ivlev*, 1955]:

$$I = R_m[1 - \exp (-\Lambda P)] \tag{40}$$

where R_m is the maximum ingestion rate of zooplankton and Λ determines the sensitivity of grazing to phytoplankton stock. Equation (40) has been modified to account for food-acclimatized grazing [*Mayzaud and Poulet*, 1978; *Franks et al.*, 1986] defining R_m such that

$$R_m = R\Lambda P \tag{41}$$

where R is a grazing rate. The nomenclature has been modified to follow Franks et al. to eliminate confusion. In their formulation, (40) would be defined as $I = R_m\ P[1 - \exp (-\Lambda P)]$. The use of the coefficient R_m is misleading, however, because this equation approaches no maximum grazing threshold but, instead, increases geometrically, then linearly, as a function of P. The equation by *Ivlev* [1955] has an asymptotic upper limit to I defined by R_m. As defined in (40), R_m is constantly changing in response to changes in P, hence its being regarded as the food-acclimatized R_m.

The carbon concentration at each depth can be calculated using

$$C = P \frac{\text{chl } a}{N} \frac{C}{\text{chl } a} \tag{42}$$

where chl a/N is assumed to be constant (a value of 1 is used) and C/chl a is computed using the equation:

$$\frac{C}{\text{chl } a} = [-390 + 395 \log (E^*)]10^{(-0.645G)} \tag{43}$$

where G has been averaged over 24 hours. Coefficients used in (43) were determined by applying a least squares regression to data from *Kiefer and Cullen* [1991].

The respiration rates for phytoplankton r_p (d^{-1}) and zooplankton r_z (d^{-1}) are defined as

$$r_p = r_{po} \exp (k_{rp}T) = \eta G_0 \exp (k_{rp}T) \tag{44}$$

$$r_z = r_{zo} \exp (k_{rz}T) \tag{45}$$

where r_{po} and r_{zo} are the respiration rates at 0°C for phytoplankton and zooplankton, respectively; k_{rp} and k_{rz} define the temperature sensitivity of r_p and r_z, respectively; and η is the ratio of phytoplankton respiration to growth. The death rates of phytoplankton m (d^{-1}) and zooplankton g (d^{-1}) are constants.

Daily production Π is calculated according to

$$\Pi = \int_0^{24} \int_0^{350} \text{GP} \frac{\text{chl } a}{N} \frac{C}{\text{chl } a} dz\, dt \tag{46}$$

and the bulk f ratio (the average f ratio in the upper 350 m of the water column) is defined as

$$f_b = \frac{\int_0^{350} \pi_2 \text{ GP } dz}{\int_0^{350} \text{GP } dz} \tag{47}$$

where 350 m is the limit of the model domain.

3. Data Set Descriptions

A variety of data sets from OWS P were used for surface forcing and for evaluation of model performance. Data types include surface meteorological time series, temperature profile time series, COADS monthly mean surface wind fields, climatological hydrographic and surface irradiance data, and biological and nutrient observations.

3.1. OWS P Surface Observation Time Series

These data include time series at 3-hour resolution of air temperature, dew point temperature, wind velocity, cloud cover, and SST for the period of January 1951 through December 1980. With the exception of SST these data were used to force the mixed layer model and compute the surface irradiance field as described above. The climatological cloud cover from the OWS P observations varies from about 6 oktas in autumn to 7.75 oktas in summer. The COADS monthly mean cloud cover climatology has a similar pattern, with slightly higher values in autumn.

3.2. Temperature Profile Time Series

For the period of January 1950 through December 1966 (excluding 1951 and most of 1952, when no data were collected), temperature profiles were routinely collected at OWS P. Generally, the sampling was at least once per day. The data were gridded at 5-m vertical resolution by investigators at the Naval Postgraduate School.

3.3. COADS Surface Wind Fields

The COADS monthly mean winds for 1951–1980 were used to compute the Ekman upwelling at OWS P (Figure 2). The Ekman vertical velocities are noticeably noisier in the earlier years. Data from the Experiment on Rapidly Intensifying Cyclones over the Atlantic (ERICA) were used to evaluate the effects of time and space averaging [*Tai and McClain*, 1992, 1993]. Monthly mean Ekman upwelling derived from objectively analyzed ERICA wind fields (6-hour intervals) were 2 to 5 times greater than (1) the values obtained from monthly mean ERICA winds and (2) mean Ekman upwelling values obtained using Fleet Numerical Oceanographic Center winds, the two cases representing the effects of coarse temporal and spatial scales. Therefore simulations were also conducted with the Ekman values amplified by a factor of 3.

3.4. Climatological Hydrographic Data

Temperature and salinity from the *Levitus* [1982] seasonal climatologies were used to check the climatology derived from the temperature profile data and to initialize the model temperature and salinity profiles. The Levitus winter temperature

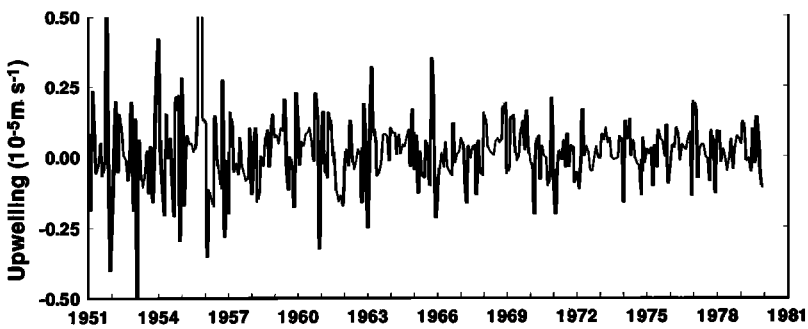

Figure 2. The 30-year time series of monthly climatological Ekman upwelling at ocean weather station (OWS) P. Wind data used to calculate Ekman upwelling were obtained from the Comprehensive Ocean-Atmosphere Data Set (COADS) [*Woodruff et al.*, 1987].

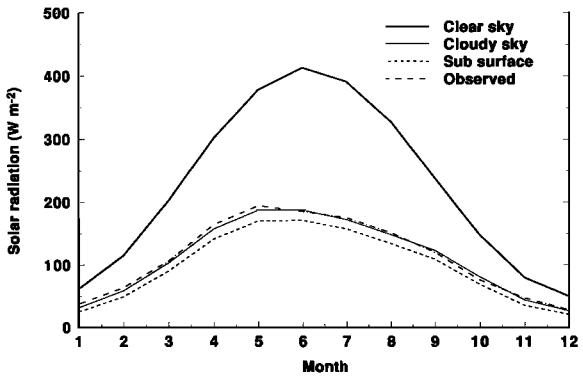

Figure 3. Monthly mean solar radiation between 250 and 4000 nm at OWS P. Data were obtained from *Dobson and Smith* [1988].

climatology was used to initialize the model because early observed profiles did not extend to 350 m, the vertical domain of the model. Below about 100 m the seasonal climatological temperatures are 4–4.5°C. The SST ranges from approximately 5°C in winter to 12.5°C in summer. The seasonal temperature profile climatologies derived from the temperature time series are nearly identical to the Levitus profiles. The Levitus seasonal salinity profiles indicate little seasonal variation. Above 100 m the range is less than 0.25‰, and below 100 m the seasonal profiles are identical. Between 100 and 150 m the salinity sharply increases by more than 1‰ for all seasons.

3.5. Biological and Nutrient Observations

A total of 148 chl *a* profiles in the vicinity of OWS P (±5° latitude and longitude) were obtained from the sea-viewing wide field-of-view sensor (SeaWiFS) historical pigment archive [*Firestone and McClain*, 1994]. The data were collected between July 1959 and July 1973. Seasonal climatological profiles show surface values ranging from 0.27 mg m^{-3} in winter to 0.42 mg m^{-3} in summer. The chl *a* profiles converge near 200 m, with a value less than 0.10 mg m^{-3}. Integrated 0- to 50-m chl *a* values were also digitized from *Frost* [1991].

Initially, NO_3 profiles were obtained from *National Oceanographic Data Center (NODC)* [1993] station data and the *Levitus et al.* [1993] annual NO_3 climatology. Only seven profiles representing two seasons (spring and fall) were found. The mean profile matched the Levitus et al. climatological profile reasonably well and indicated a nearly linear increase in NO_3 from about 10 mg-at m^{-3} at the surface to 40 mg-at m^{-3} at 350 ms. In an effort to estimate the climatological profiles for each season, additional data were obtained from NODC for the region within 5° of OWS P. This data set included over 5000 hydrocasts, with only 47 casts containing NO_3 profiles. These data were used for comparisons with the simulated NO_3 profiles. Integrated 0- to 50-m NO_3 concentration data were digitized from *Frost* [1991].

4. Results

4.1. Heat Fluxes

The observed incident short wave radiation at OWS P ranged from about −25 W m^{-2} in winter to −250 W m^{-2} in summer during 1960–1961 [*Ashburn*, 1963]. The climatological monthly mean values, simulated and observed [*Dobson and Smith*, 1988], are shown in Figure 3 and are compared with the clear sky irradiances. The monthly mean long wave radiation varied from about 25 (July) to 50 (November) W m^{-2}. The latent heat flux has the greatest seasonality, with a climatological minimum in July of about 15 W m^{-2} and a maximum of 95 W m^{-2} in October. Similarly, the range for the sensible flux was −5 W m^{-2} in July to 25 W m^{-2} in November. Figure 4

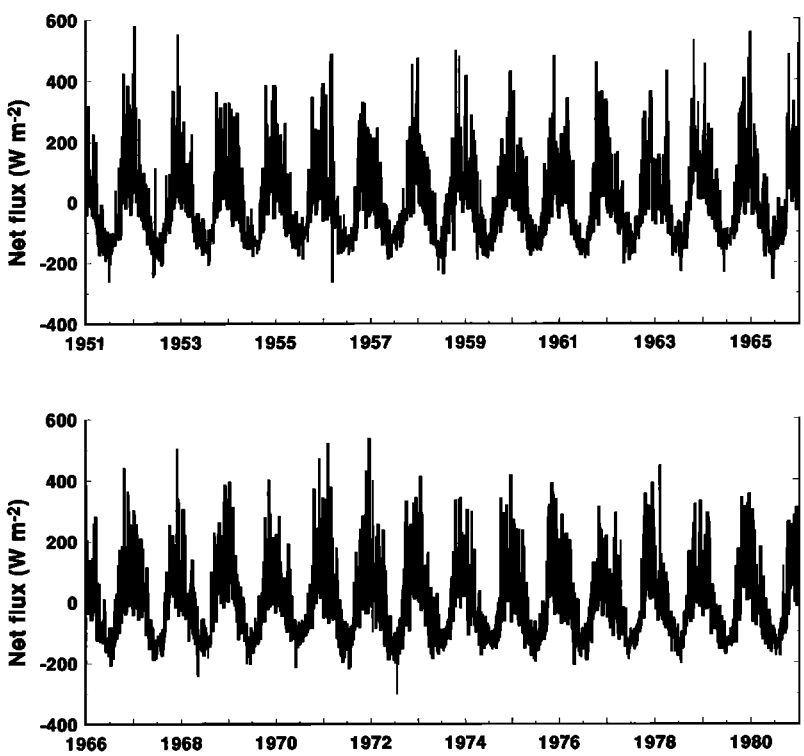

Figure 4. The 30-year time series of net energy flux at OWS P.

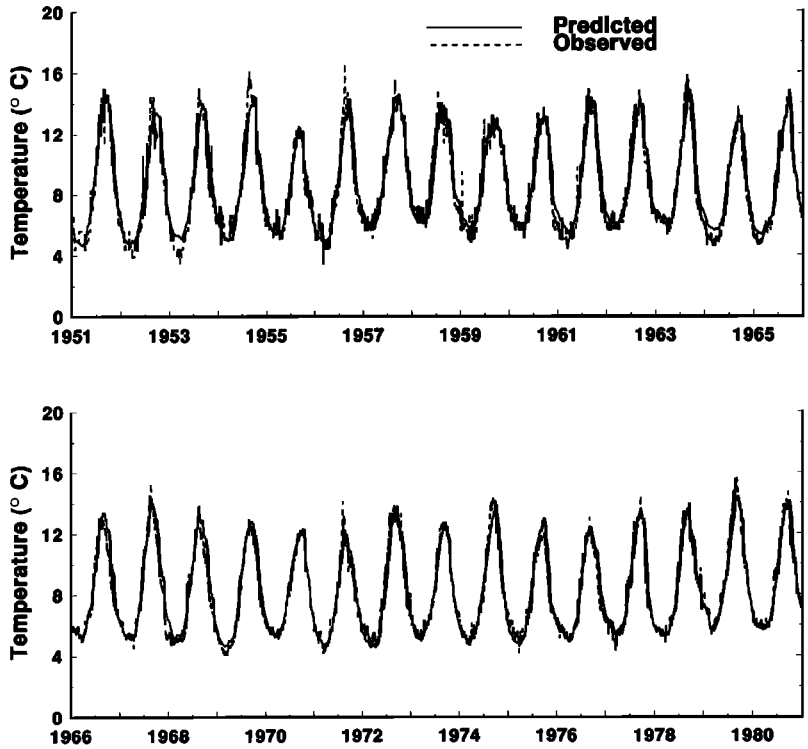

Figure 5. The 30-year time series of predicted and observed sea surface temperature at OWS P. Observational data were obtained from the data archive at the National Center for Atmospheric Research, Boulder, Colorado.

shows the 30-year net flux time series which indicates a seasonal cycle of ± 150 W m^{-2}.

4.2. Temperature and Mixed Layer Depth

The predicted and observed 30-year time series of SST are shown in Figure 5. The climatological differences (simulated minus observed) range from -0.4°C in summer to 0.7°C in fall. The seasonal biases in SST as derived from the profile data (Figure 6) show the greatest positive difference in winter rather than autumn. *Archer et al.* [1993] and *Large et al.* [1994] have observed similar differences between modeled and observed temperatures at OWS P during the winter and suggest horizontal advection as the cause. Nonetheless, the simulated profiles are within 1 standard deviation of the mean in all seasons and at all depths.

Both the predicted and observed (1953–1966 only) MLDs exhibited a great deal of interannual variability during the winter (Figure 7), ranging from 110 to >200 m. Unrestricted, the simulated MLDs were too shallow in the summer, making it necessary to impose a minimum value (30 m). The observed summertime minimum MLD ranged from 25 to 30 m. Also, the model MLDs tended to shallow about a month too soon in spring and deepen a month too late in fall. The wintertime model MLDs were very close to the observed values.

4.3. Eddy Diffusion Coefficient

Figure 8 shows the climatological monthly profiles of K_v. As expected, the values are highest in winter when the wind stress and MLD are greatest. Wintertime stresses were typically 0.5 to 1.0 nt m^{-2} (where nt is newtons), but values as high as 4 nt m^{-2} were recorded. July had the lowest values at all depths.

4.4. Phytoplankton

Average concentrations of chl *a* in the upper 50 m of the water column remained relatively constant throughout the year (Figure 9), varying from an autumn peak of approximately 0.34 mg m^{-3} to a late spring minimum of 0.20 mg m^{-3}. A secondary early spring peak ranging from 0.26 to 0.30 mg m^{-2} was often present following a winter decline in phytoplankton biomass. Interannual variation of this pattern was very small.

Vertical distributions of chl *a* predicted by the model remained relatively constant throughout the year (Figure 10). In the upper 50 m of the water column, concentrations of chl *a* were generally uniform, except in midsummer when surface waters were more strongly stratified, ranging seasonally from 0.2 (spring) to 0.3 mg m^{-3} (autumn). Between the depths of 50 and 200 m, chl *a* exhibited a gradual decline to approximately 0.05 mg m^{-3}, regardless of season.

4.5. Microzooplankton

Like chl *a*, the annual cycle of microzooplankton biomass exhibited very little interannual variation (Figure 9). Average concentrations in the upper 50 m were greatest in midsummer (0.60 mg-at N m^{-3}) and lowest in midwinter (0.20 mg atm N m^{-3}), tracking the temporal pattern in primary production. The rate of microzooplankton grazing was in phase with phytoplankton growth rate and primary production, being greatest in the late summer and least in late winter.

4.6. Gross Primary Production and New Production

Predicted gross and new primary production in the upper 50 m (Figure 11) exhibited a regular temporal pattern that was related to the annual cycle of solar radiation (Figure 3). Gross

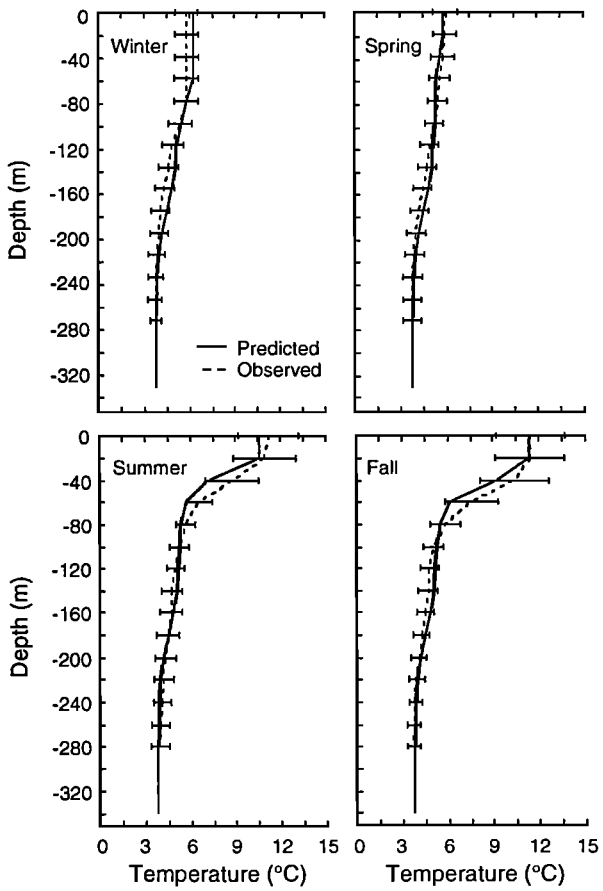

Figure 6. Comparison of predicted and observed climatological seasonal temperature profiles at OWS P. Observational data were obtained from D. Adamec, NASA Goddard Space Flight Center.

production typically ranged from 0.05 g C m^{-2} d^{-1} during the winter months to 1.0 g C m^{-2} d^{-1} in summer. Similarly, rates of new production ranged seasonally from 0.03 to 0.40 g C m^{-2} d^{-1}. Gross primary production was highest near the ocean surface, reaching >1.5 mg C m^{-3} d^{-1} in August and September, and decreased exponentially with depth, similar to the pattern exhibited by in-water radiation. The annual rate of new production, which is equivalent to the production exported from the euphotic zone, and gross production (Figure 12) ranged from 78 to 83 g C m^{-2} yr^{-1} and from 182 to 196 g C m^{-2} yr^{-1}, respectively.

4.7. Nitrate and Ammonium Concentrations

Average NO_3 concentration in the upper 50 m of the water column showed marked seasonal and interannual variability (Figure 13). Over an annual cycle, NO_3 concentrations generally ranged from 6 mg-at m^{-3} in mid-September to 15 mg-at m^{-3} in mid-March. However, the magnitude of the spring NO_3 maximum varied interannually between 10 and 23 mg-at m^{-3}. Similarly, the autumn minimum ranged from 1 to 12 mg-at m^{-3}. As expected, the autumn decline in surface NO_3 coincided with the peak in phytoplankton abundance. The lowest NO_3 values occurred in 1962 when the winter mixed layer was very shallow and the Ekman upwelling was not decidedly upwelling or downwelling. Generally, the magnitude of the annual NO_3 cycle varied as a function of Ekman upwelling. Simulations where w_e was increased by a factor of 3 exhibited marked changes in NO_3 in the upper 50 m of the water column. For example, near-complete NO_3 exhaustion was observed during late summer 1956–1958 when the surface winds were predominantly downwelling favorable. Surprisingly, even in the standard simulation, large fluctuations and even near depletion

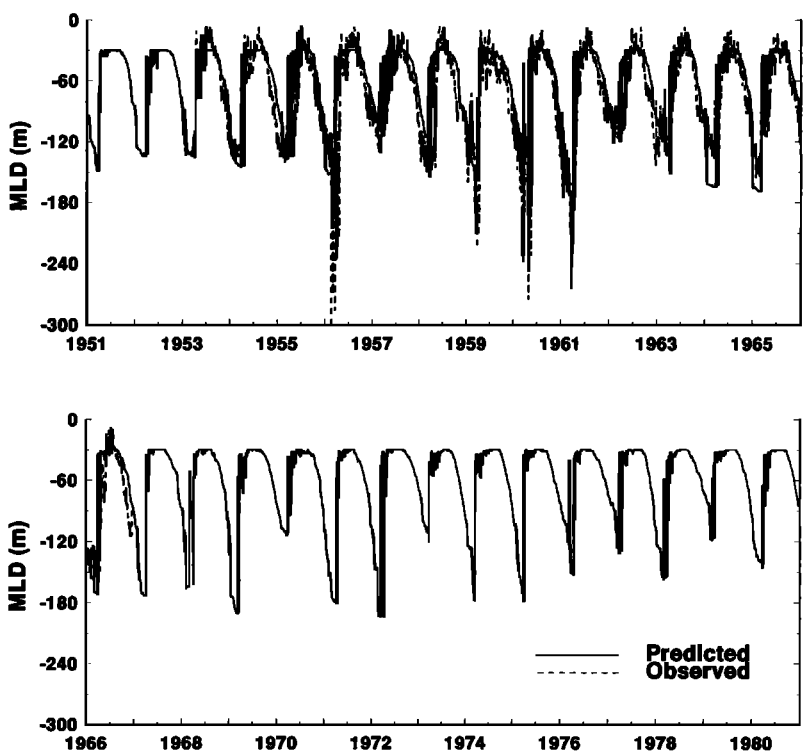

Figure 7. Time series of 30-year predicted and 14-year (1953–1967) observed mixed layer depth (MLD) at OWS P. MLD was determined from temperature profiles provided by D. Adamec, NASA Goddard Space Flight Center.

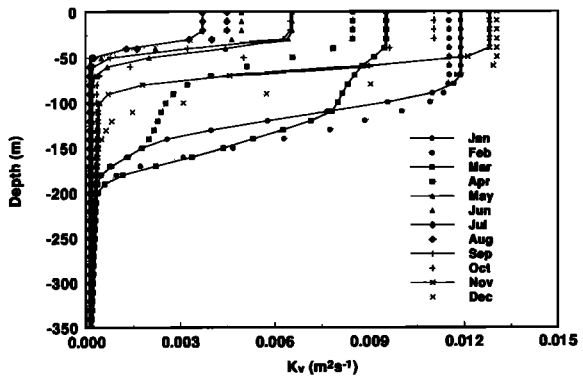

Figure 8. Monthly climatological eddy diffusivity K_v profiles at OWS P predicted by the model.

of NO_3 (e.g., 1962) produced only small variations in annual primary production (Figure 12).

Like NO_3, the average NH_4 concentration in the upper 50 m of the water column showed both marked seasonal and interannual variability (Figure 13), although the annual pattern was 180° out of phase with respect to nitrate. Concentrations typically reached their minimum of 0.15 mg-at m^{-3} in March, although this minimum value ranged from 0.125 to 0.250 mg-at m^{-3}. This is somewhat higher than the near depletion of NH_4 observed in the summer months during the SUPER cruises (1993). Peak NH_4 concentrations were predicted in December and varied annually from 0.30 to 0.40 mg-at m^{-3}, consistent with observations from *Frost* [1993].

Despite the high ambient NH_4 concentrations, the predicted bulk f ratio ranged seasonally from 0.3 to 0.6, demonstrating that a substantial proportion of N demand was satisfied by NO_3. As expected, the autumn minimum coincided with both the high rates of primary productivity, which resulted in reduced NO_3 abundance, and the maximum rate of secondary productivity, which led to the release of large amounts of NH_4. The high f ratios in late winter and early spring reflect the high concentrations of NO_3 brought to the surface during winter mixing and the low production of NH_4 by the microzooplankton population.

5. Discussion

5.1. Phytoplankton Standing Crop

Model predictions of vertical chl *a* distribution are in good agreement with in situ profiles, despite the fact that the observed chl *a* data are highly variable with respect to depth (Figure 10). Vertical gradients in chl *a* were maintained in the model by the relatively high phytoplankton growth rates in the upper water column. From February to September the rate of phytoplankton growth exceeded losses from sinking and zooplankton grazing, and surface concentrations remained relatively constant. At depths >100 m both predicted and observed chl *a* concentrations were greatest (up to 0.2 mg m^{-3}) between December and March. This timing reflects a balance between modest phytoplankton growth rates at a time of relatively short photoperiod and light intensity, low grazing pressure, and high vertical mixing. By midsummer, mixing was low, zooplankton stocks had built up, grazing exceeded phytoplankton growth at depth, and chl *a* was reduced to less than 50% of the spring peak.

The predicted annual pattern of phytoplankton biomass agrees well with in situ chl *a* data collected at OWS P which show that phytoplankton standing crop exhibits only a modest annual cycle (Figure 14a). Observations also indicate that substantial high-frequency variation in chl *a* exists at OWS P

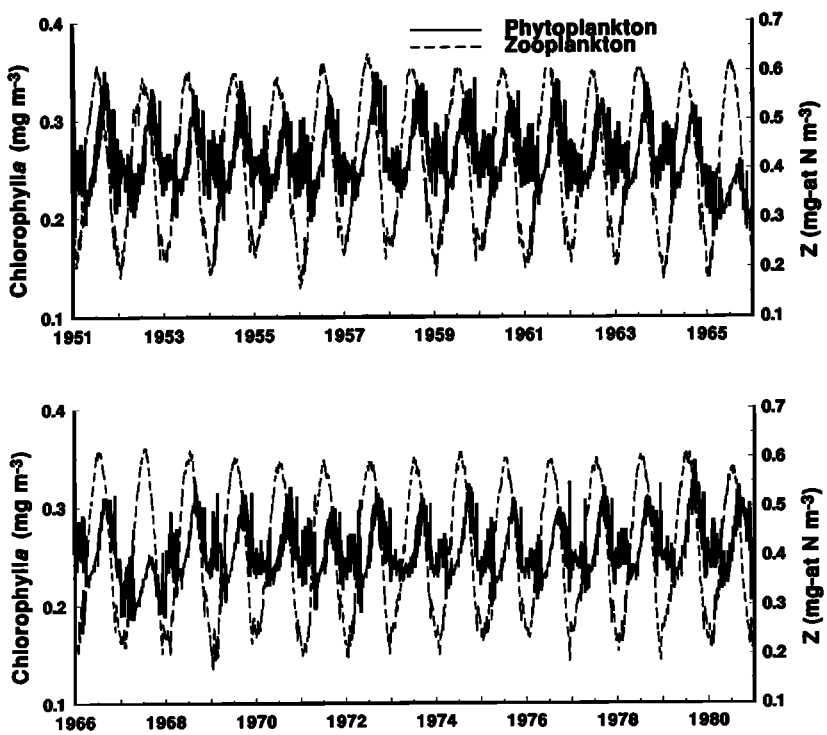

Figure 9. The 30-year time series of simulated mean surface (0–50 m) chlorophyll *a* and zooplankton nitrogen.

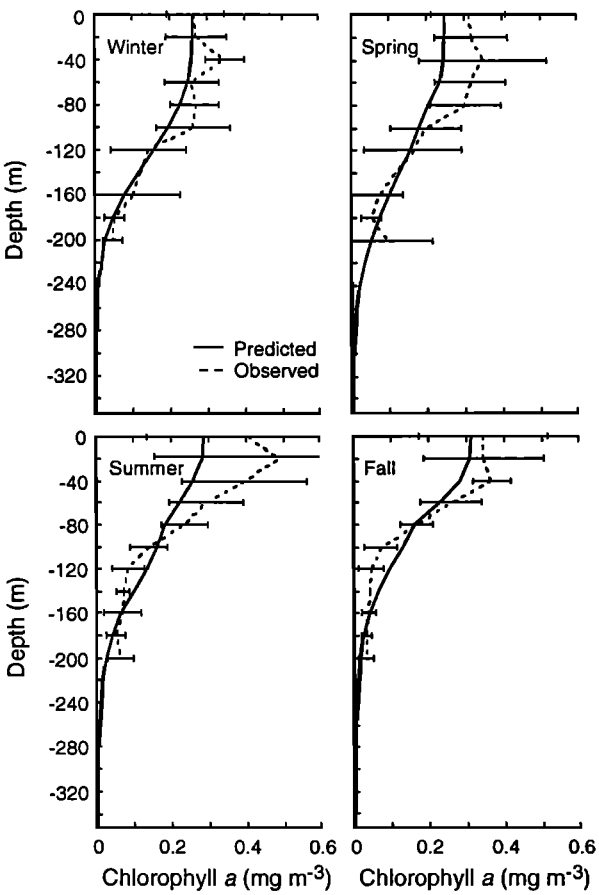

Figure 10. Comparison of predicted and observed climatological seasonal chlorophyll *a* profiles. Observational data were obtained from *Firestone and McClain* [1994].

[*Welschmeyer et al.*, 1991], and our model results support that conclusion. Previous models [*Frost*, 1993] suggest that this variability is due to changes in MLD. However, when MLD was held constant during the summer months in our simulations, the high-frequency variations in chl *a* persisted, suggesting that variability in daily insolation is responsible.

Some recent evidence indicates that phytoplankton pigment concentrations in the subtropical Pacific Ocean have increased over the last few decades [*Venrick et al.*, 1987], although this is still a matter of debate [*Falkowski and Wilson*, 1992]. However, model results show no evidence of a long-term increase in phytoplankton standing crop at OWS P like that observed farther south in the central North Pacific gyre by *Venrick et al.* [1987]. Because the model was forced with high-frequency observational data for the years 1951–1980, certain interannual differences in the forcing data would have resulted in changes in phytoplankton standing crop. Our analysis of 30 years of meteorological data and its predicted effect on biological processes at OWS P reveal no decadal trends in surface heat fluxes, cloud cover, winds, SST, phytoplankton, zooplankton, or nutrient fields. Interannual variability is most evident in the MLD, but changes in this variable do not have a significant effect on annual primary productivity. If pigments have increased over the last few decades, the increase cannot be due to local forcing, but must be a result of a large-scale shift in water mass boundaries or a change in the influx of trace nutrients such as iron from atmospheric dust. Model results for the case where Ekman was amplified by a factor of 3 did show that NO_3 can be nearly depleted during periods of either shallow winter MLDs or periods of persistent downwelling. Therefore local atmospheric forcing of mixing and Ekman upwelling cannot increase productivity, but only decrease it. Also, the monthly climatological cloud cover fraction is fairly constant throughout the year at about 0.8 and would need to decrease

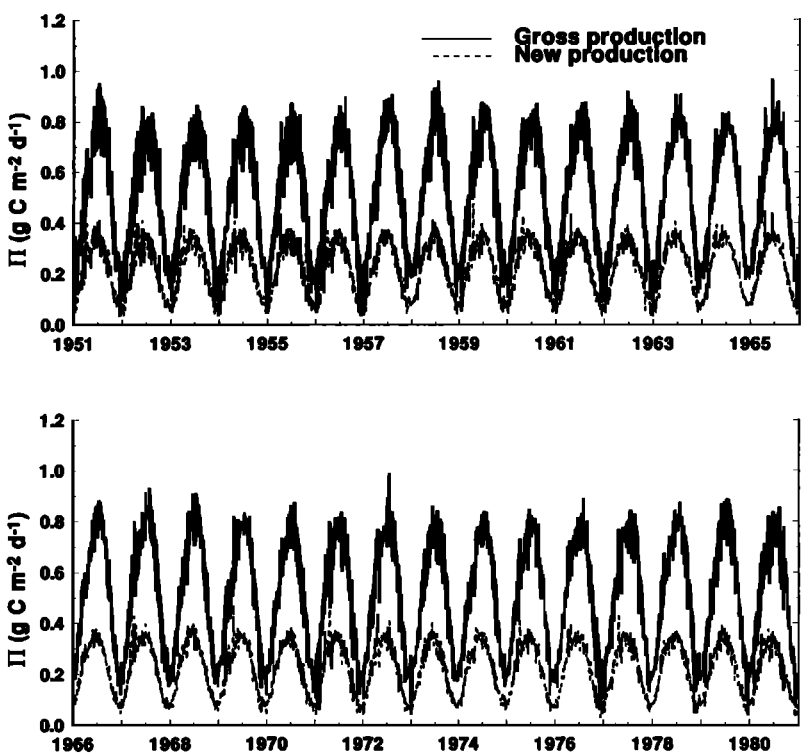

Figure 11. The 30-year time series of simulated surface (0–50 m) gross and new production.

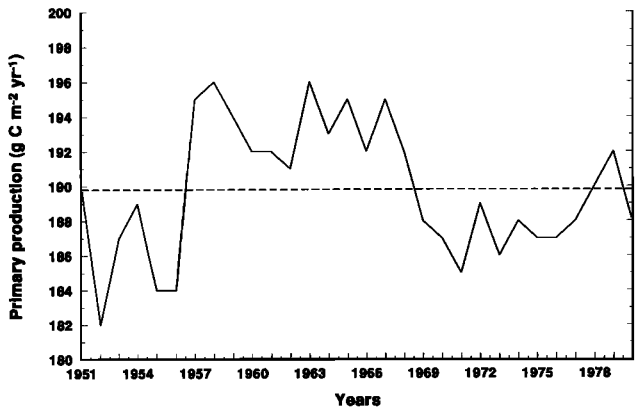

Figure 12. The 30-year time series of predicted annual primary production.

substantially to have any impact on surface irradiance, e.g., a decrease in cloud cover from 0.8 to 0.6 results in only a 6% increase in E_{surf} (equation (5)). The absence of predicted interannual variation in chl *a* at OWS P suggests that variation in local forcing was too small to affect phytoplankton biomass in the manner observed by *Venrick et al.* [1987].

5.2. Primary Production at OWS P

Historically, OWS P has been considered to be a region of low primary productivity, with annual rates estimated to be in the range of 30 to 60 g C m^{-2} yr^{-1} [*McAllister*, 1972; *Frost*, 1987] (Table 2). These estimates were supported by the low phytoplankton standing crops and the high nutrient concentrations characteristic of the sub-Arctic Pacific. However, more recent in situ measurements of primary production made using clean ^{14}C techniques suggest that primary production may actually be two- or threefold higher (140–170 g C m^{-2} yr^{-1}) than previously thought [*Wong et al.*, 1995; *Welschmeyer et al.*, 1993].

The annual production rate predicted by the model (approximately 190 ± 8 g C m^{-2} yr^{-1}) supports the notion that OWS P is a region of high productivity. Predicted average daily rates of production over the entire year were approximately 521 mg C m^{-2} d^{-1}, in good agreement with recent estimates (Figure 14b). In addition, the predicted productivity between May and August (600–800 mg C m^{-2} d^{-1}) is consistent with the average of 631 mg C m^{-2} d^{-1} reported by *Welschmeyer et al.* [1991] and the range of 250–750 mg C m^{-2} d^{-1} (calculated from new production estimates of 100–300 mg C m^{-2} d^{-1} divided by the f ratio of 0.4) given by *Emerson* [1987]. Moreover, *Martin et al.* [1989] and *Welschmeyer et al.* [1991] measured maximum summer rates of production in excess of 1000 and 1300 mg C m^{-2} d^{-1}, respectively, 3 times greater than the highest rates reported previously. Typical summer peaks predicted by the model ranged between 900 and 1000 mg C m^{-2} d^{-1}.

However, while the model estimate of integrated annual production agrees well with recent studies [*Berger et al.*, 1989; *Welschmeyer et al.*, 1991; *Falkowski and Wilson*, 1992; *Wong et al.*, 1995], the annual cycle of production differs from that presented by *Wong et al.* [1995] in important ways. The most obvious difference is that the model predicts higher rates of production in summer and lower rates in winter. The data presented by *Wong et al.* [1995] show summer rates of production (466 mg C m^{-2} d^{-1}) that are only 64% higher than winter rates (283 mg C m^{-2} d^{-1}). In contrast, average summer rates of production predicted by the model (600–800 mg C m^{-2} d^{-1}) are more than fourfold higher than minimum winter rates (150 mg C m^{-2} d^{-1}).

The only available data for winter production at OWS P using clean incubation techniques are given by *Wong et al.* [1995]. Their estimates of production were based on rates

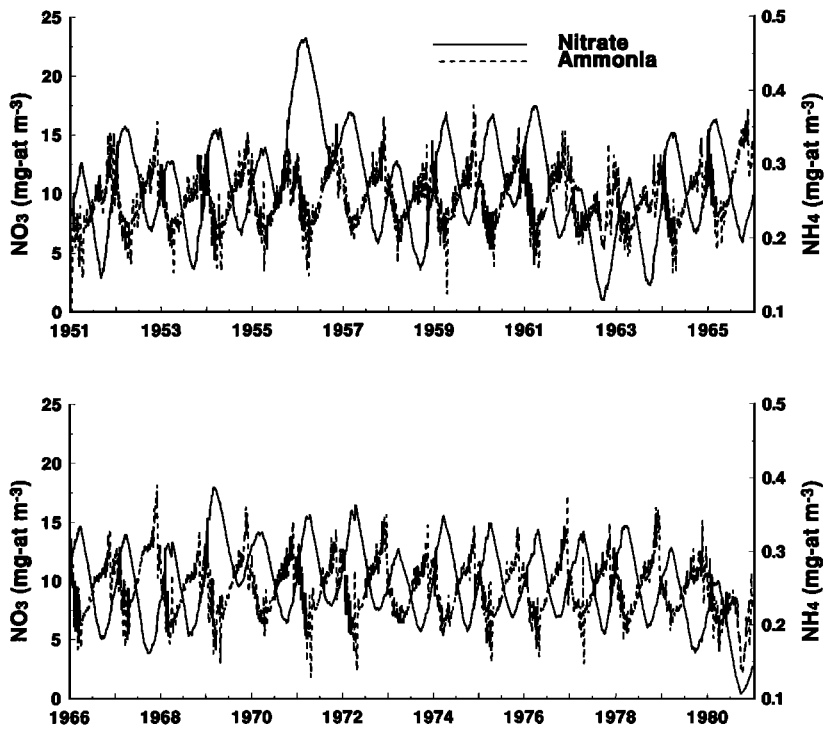

Figure 13. The 30-year time series of simulated mean surface (0–50 m) nitrate and ammonium concentrations.

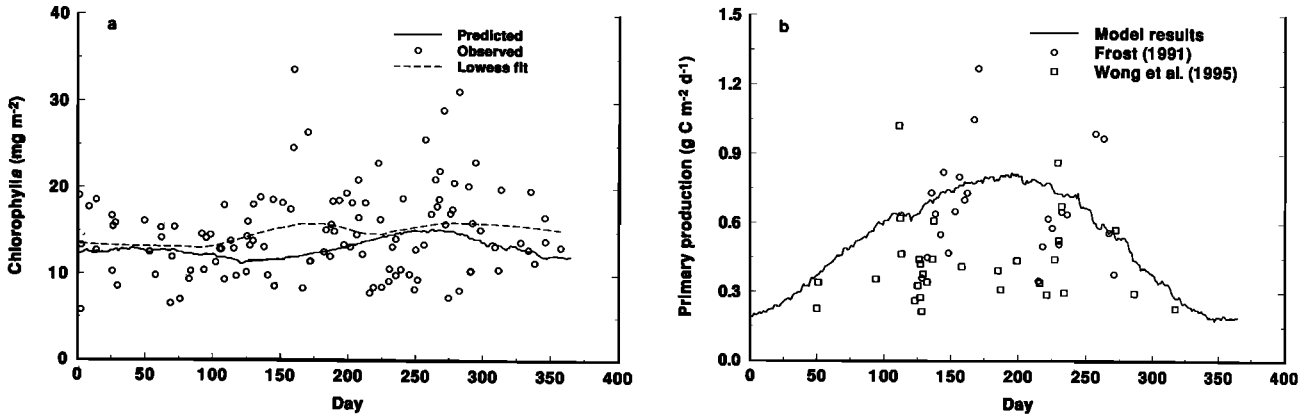

Figure 14. Comparison of predicted and observed annual cycles of surface (0–50 m) (a) chlorophyll *a* and (b) gross primary production. Observational data were obtained from *Frost* [1991] and *Wong et al.* [1995]. The lowess line represents a curve fit to the observational data.

measured between dawn and noon which were extrapolated over the entire day. Because they assumed respiration was less than 15% of daily gross production, nighttime respiration was ignored, regardless of season. However, because the dark cycle is much longer during the winter (16 hours on December 21) than it is in summer (8 hours on June 21), nighttime respiration would be expected to be relatively greater in winter, resulting in reduced net production. Although it could be argued that cold winter temperatures may compensate for the longer night and keep respiration low in winter, this is doubtful, given the fact that low winter temperatures did not unduly suppress rates of gross primary production. It is well known that phytoplankton have a variety of mechanisms which allow them to partially maintain their photosynthetic rates at reduced temperatures [*Li*, 1980; *Li and Morris*, 1982; *Li et al.*, 1984], and it is also known that rates of respiration are higher when photosynthetic rates increase. Therefore because respiration was neglected during their study, it is likely that *Wong et al.* [1995] have overestimated rates of primary production in the winter.

However, it is unlikely that nighttime respiration alone can explain the differences between the modeled rates of winter production and those reported by *Wong et al.* [1995]. The strong annual signal predicted by the model was induced primarily by seasonal changes in photoperiod and light intensity and less so by rates of respiration. Because primary production is the product of the phytoplankton standing crop and its growth rate, it is curious that observed patterns of photosynthesis [*Wong et al.*, 1995] are not more tightly coupled to the annual light cycle, particularly because nutrients do not limit the photosynthetic rate, and the phytoplankton standing crop changes little with season. If winter production rates really are as high as those reported by *Wong et al.* [1995], they must reflect either the ability of the phytoplankton population to photoacclimate to reduced light intensities during the summer-winter transition or a shift in species composition from a high light-acclimated assemblage in the summer to a low light assemblage in the winter. This latter explanation is supported by *Venrick* [1993], who has found distinct surface and deep water phytoplankton assemblages in the central North Pacific Ocean near 29°N, 154°W.

A seasonal change in the taxonomic composition of the surface phytoplankton assemblage was incorporated into the model by varying the value of $I_{k\max}$ as a function of MLD. In winter, when MLDs exceeded 60 m, $I_{k\max}$ was set to 25 μE m^{-2} s^{-1}. When the MLD shoaled in spring and summer to <60 m, $I_{k\max}$ was increased to 250 μE m^{-2} s^{-1}. An alternative approach would be to modulate $I_{k\max}$ as a sine function with season. The former method was chosen, however, because it more adequately simulated the mixing of deep water phytoplankton populations to the surface in winter as proposed by *Venrick* [1993]. Results of this simulation were very similar to those obtained in the standard simulation. However, when the MLD exceeded 60 m, the reduced $I_{k\max}$ resulted in higher primary productivity rates in the winter and slightly greater phytoplankton and zooplankton standing crops. When the MLD was <60 m, the higher values for $I_{k\max}$ resulted in a slight reduction in phytoplankton biomass and a 25% drop in zooplankton abundance in the summer. These results suggest that the seasonally stable phytoplankton standing crop at OWS P could result from species succession, whereby deep water species dominate in the winter when mixed layers are deep and shallow water assemblages dominate in the summer when the water column is more stratified.

The high rates of production and high f ratios suggest that the region around OWS P may be a more important compo-

Table 2. Estimates of Annual Primary Production at Ocean Weather Station P

Production, g C m^{-2} yr^{-1}	Comment	Reference
34	modeled	*Frost* [1987]
60	measured	*McAllister* [1972]
>113	measured*	*Welschmeyer et al.* [1991]
140	measured	*Wong et al.* [1995]
54–180	climatology	*Koblents-Mishke et al.* [1970]
162	modeled	*Frost* [1993]
170	measured	*Welschmeyer et al.* [1993]
189	estimated from Secchi data†	*Falkowski and Wilson* [1992]
190	modeled	this study
193	empirical model	*Eppley et al.* [1985]
60–200	climatology	*Berger et al.* [1989]

*Measured May–October only.
†North Pacific Ocean.

nent of the carbon cycle than previously thought. These rates are comparable to rates of new production reported for upwelling regions in the eastern Pacific Ocean [*Martin et al.*, 1989] and the equatorial Pacific Ocean [*Chavez and Barber*, 1987], which have higher rates of GP but lower f ratios. Export production from OWS P is also more than twofold higher than the coastal northeast Pacific Ocean and four- to fivefold greater than the central Pacific Ocean [*Martin et al.*, 1989]. However, because phytoplankton and zooplankton biomass at OWS P is dominated by small size classes which presumably sink very slowly, it is unclear what fraction of the exported production reaches the deep ocean. The primary biogenic loss from the upper 350 m in the model is from fecal pellet production which is assumed to be permanent. The extent to which this is true will determine how important OWS P is as a sink for atmospheric CO_2.

5.3. Microzooplankton

The predicted rapid response by zooplankton to changes in food abundance is consistent with a population dominated by heterotrophic microzooplankton, which have high mass-specific metabolic rates and high intrinsic growth rates when compared to heterotrophic metazoans such as copepods, krill, and gelatinous zooplankton [*Frost*, 1987]. Zooplankton with distinct reproductive cycles such as planktonic crustaceans do not respond numerically to sudden increases in food supply. There is little evidence that individual microzooplankton can vary their digestive enzyme concentrations in response to increased food supply (food acclimation) as has been observed for copepods [*Mayzaud and Poulet*, 1978]. However, because phytoplankton standing crop remains relatively constant throughout our simulations, little food acclimation by the microzooplankton is necessary.

5.4. Nutrients

The long term stability of NO_3 in the upper 50 m, particularly in winter, is an important feature of the model and shows excellent agreement with observations (Figure 15) including vertical profiles (Figure 16). The nitrate balance can be obtained by combining terms in (24a)–(24d) (note that $m = 0$ in Table 1) and integrating over the depth of the model domain for 30 years, yielding

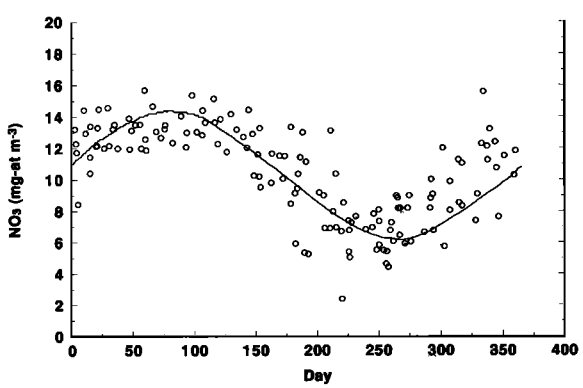

Figure 15. Comparison of predicted and observed annual cycles of mean surface (0–50 m) nitrate. Observational data were obtained from *Frost* [1991].

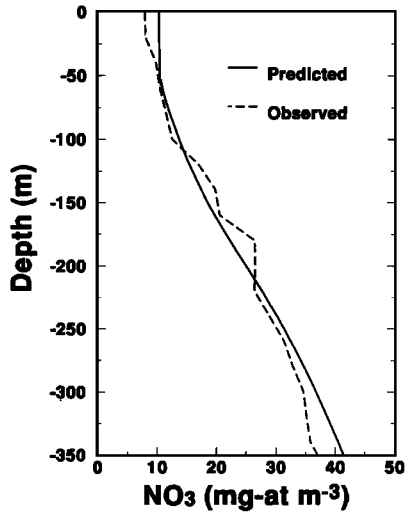

Figure 16. Comparison of observed and simulated climatological nitrate profiles. The observed climatology was derived by averaging the seasonal climatologies so as to remove sampling bias. Observational data were obtained from the National Oceanographic Data Center.

$$\frac{1}{30\text{ years}}\int_0^{30\text{ years}}\int_0^{350}\frac{\partial N}{\partial t}\,dz\,dt \approx \frac{1}{30\text{ years}}$$

$$\cdot\int_0^{30\text{ years}}\int_0^{350}\left[-w_e\frac{\partial NO_3}{\partial z}+\frac{\partial}{\partial z}\left(K_v\frac{\partial NO_3}{dz}\right)\right.$$

$$\left.-g(1-az)Z-rIZ\right]dz\,dt \approx (0.93+5.97$$

$$-2.15-4.58)\times 10^{-4}\text{ mg-at N m}^{-2}\text{ s}^{-1} \qquad (48)$$

The terms not shown on the right-side of the equation have magnitudes $<0.2\times 10^{-4}$ mg-at N m^{-2} s^{-1}. It has been suggested that the residual NO_3 at the end of the summer provides a buffer against winters with few storm events and little mixing [*Miller et al.*, 1991]. If this residual NO_3 were to be used up and winter mixing did not restore concentrations to their usual high levels, there might be insufficient nitrate to drive the system the following spring. As noted by *Frost* [1991], however, only a few brief but intense mixing events may be needed to restore NO_3 concentrations to their winter levels. The model results demonstrate that during the 30 years of our simulation, winter mixing, which is driven by wind speed in the model, was consistently sufficient to fully restore NO_3 in the upper 50 m of the water column. These results suggest that the probability of winter storms being too weak to drive deep mixing is small.

Acknowledgments. We are grateful to Michele Reineker and David Adamec for their helpful discussions about eddy diffusion. We also thank David Adamec for providing us with temperature data and those individuals at the Naval Postgraduate School who processed the data. We wish to acknowledge the four reviewers for their comprehensive comments which were most useful in refining the manuscript. This work was supported under NASA RTOP 579-11-01-01 to C.R.M. and NASA RTOP 579-11-07 to K.R.A.

References

Archer, D., E. Emerson, T. Powell, and C. S. Wong, Numerical hindcasting of sea surface pCO_2 at Weathership Station Papa, *Prog. Oceanogr.*, *32*, 319–351, 1993.

Arrigo, K. R., and C. W. Sullivan, A high resolution bio-optical model of microalgal growth: Tests using sea ice algal community time series data, *Limnol. Oceanogr.*, *39*, 609–631, 1994.

Ashburn, E. V., The radiative heat budget at the ocean-atmosphere interface, *Deep Sea Res.*, *10*, 597–606, 1963.

Austin, R. W., The remote sensing of spectral radiance from below the ocean surface, in *Optical Aspects of Oceanography*, edited by N. G. Jerlov and E. Steeman Nielsen, pp. 317–344, Academic, San Diego, Calif., 1974.

Baker, K. S., and R. C. Smith, Bio-optical classification and model of natural waters, 2, *Limnol. Oceanogr.*, *27*, 500–509, 1982.

Berger, W. H., V. S. Smetacek, and G. Wefer (Eds.), *Productivity of the Ocean: Present and Past*, 471 pp., John Wiley, New York, 1989.

Berliand, M. E., and T. G. Berliand, Determining the net long-wave radiation of the Earth with consideration of the effect of cloudiness, *Izv. Akad. Nauk SSSR Ser. Geofiz.*, *1*, 1952.

Budyko, M. I., *Climate and Life*, 508 pp., Academic, San Diego, Calif., 1974.

Chavez, F. P., and R. T. Barber, An estimate of new production in the equatorial Pacific, *Deep Sea Res., Part A*, *34*, 1229–1243, 1987.

Chen, D., L. M. Rothstein, and A. J. Busalacchi, A hybrid vertical mixing scheme and its application to tropical ocean models, *J. Phys. Oceanogr.*, *24*, 2156–2179, 1994.

Chriswell, S. M., E. Firing, D. Karl, R. Lukas, and C. Winn, Hawaii Ocean Time-series Program, *Data Rep. 1, 1988–1989*, 269 pp., School of Ocean and Earth Sci. and Technol., Univ. of Hawaii at Manoa, Honolulu, 1990.

Clemons, M. J., and C. B. Miller, Blooms of large diatoms in the oceanic, subarctic Pacific, *Deep Sea Res., Part A*, *31*, 85–95, 1984.

Csanady, G. T., *Circulation in the Coastal Ocean*, 279 pp., D. Reidel, Norwell, Mass., 1982.

Denman, K. L., and M. Miyake, Upper layer modification at Ocean Station *Papa*: Observations and simulation, *J. Phys. Oceanogr.*, *3*, 185–196, 1973.

Dobson, F. W., and S. D. Smith, Bulk models of solar radiation at sea, *Q. J. R. Meteorol. Soc.*, *114*, 165–182, 1988.

Dugdale, R. C., and J. J. Goering, Uptake of new and regenerated forms of nitrogen in primary production, *Limnol. Oceanogr.*, *12*, 196–206, 1967.

Emerson, S., Seasonal oxygen cycles and biological new production in surface waters of the subarctic Pacific Ocean, *J. Geophys. Res.*, *92*, 6535–6544, 1987.

Eppley, R., Temperature and phytoplankton growth in the sea, *Fish. Bull.*, *70*, 1063–1085, 1972.

Eppley, R. W., and B. J. Peterson, Particulate organic matter flux and planktonic new production in the deep ocean, *Nature*, *282*, 677–680, 1979.

Eppley, R. W., E. Stewart, M. R. Abbott, and U. Heyman, Estimating ocean primary production from satellite chlorophyll: Introduction to regional differences and statistics for the Southern California Bight, *J. Plankton Res.*, *7*, 57–70, 1985.

Eslinger, D. L., and R. Iverson, The effects of convective and wind-driven mixing on plankton dynamics, I, The southeastern Bering Sea shelf, *Cont. Shelf Res.*, in press, 1996.

Evans, G. T., and J. S. Parslow, A model of annual plankton cycles, *Biol. Oceanogr.*, *3*(3), 327–347, 1985.

Falkowski, P. G., and C. Wilson, Phytoplankton productivity in the North Pacific ocean since 1990 and implications for absorption of anthropogenic CO_2, *Nature*, *358*, 741–743, 1992.

Fasham, M. J. R., H. W. Ducklow, and S. M. McKelvie, A nitrogen-based model of plankton dynamics in the oceanic mixed layer, *J. Mar. Res.*, *48*, 591–639, 1990.

Firestone, J. K., and C. R. McClain, The historical pigment database, in *The SeaWiFS Bio-Optical Archive and Storage System (SeaBASS)*, part 1, edited by S. B. Hooker, C. R. McClain, J. K. Firestone, T. L. Westphal, E. Yeh, and Y. Ge, *NASA Tech. Memo. 104566*, vol. 20, pp. 16–22, 1994.

Franks, P. J. S., J. S. Wroblewski, and G. R. Flierl, Behavior of a simple plankton model with food-level acclimation by herbivores, *Mar. Biol.*, *91*, 121–129, 1986.

Frost, B. W., Grazing control of phytoplankton stock in the open subarctic Pacific Ocean: A model assessing the role of mesozooplankton, particularly the large calanoid copepods Neocalanus spp., *Mar. Ecol. Prog. Ser.*, *39*, 49–68, 1987.

Frost, B. W., The role of grazing in nutrient-rich areas of the open ocean, *Limnol. Oceanogr.*, *36*, 1616–1630, 1991.

Frost, B. W., A modeling study of the processes regulating plankton standing stock and production in the open subarctic Pacific Ocean, *Prog. Oceanogr.*, *32*, 101–135, 1993.

Frouin, R., D. W. Lingner, C. Gautier, K. S. Baker, and R. Smith, A simple analytical formula to compute clear sky total and photosynthetically available solar irradiance at the ocean surface, *J. Geophys. Res.*, *94*, 9731–9742, 1989.

Garwood, R. W., An oceanic mixed-layer model capable of simulating cyclic states, *J. Phys. Oceanogr.*, *7*, 455–471, 1977.

Glover, D. M., J. S. Wroblewski, and C. R. McClain, Dynamics of the transition zone in coastal zone color scanner-sensed ocean color in the North Pacific during oceanographic spring, *J. Geophys. Res.*, *99*, 7501–7511, 1994.

Ivlev, V. S., *Experimental Ecology of the Feeding of Fishes*, 302 pp., Pischepromazat, Moscow, 1955.

Janowitz, G. S., and D. Kamykowski, An Eulerian model of phytoplankton photosynthetic response in the upper mixed layer, *J. Plankton Res.*, *13*, 983–1002, 1991.

Kiefer, D. A., and J. J. Cullen, Phytoplankton growth and light absorption as regulated by light, temperature, and nutrients, *Polar Res.*, *10*(1), 163–172, 1991.

Knap, A. H., et al., Bermuda Atlantic Time-series Study data report for BATS 1–BATS 12, October 1988–September 1989, report, 268 pp., U. S. Joint Global Ocean Flux Study Plann. and Coord. Off., Woods Hole, Mass., 1991.

Koblents-Mishke, O. I., V. V. Volkovinsky, and Y. G. Kabanova, Plankton primary production of the world ocean, in *Scientific Exploration of the South Pacific*, edited by W. Wooster, pp. 183–193, Natl. Acad. of Sci., Washington, D. C., 1970.

Koepke, P., Effective reflectance of oceanic whitecaps, *Appl. Opt.*, *23*, 1816–1824, 1984.

Kremer, J. N., and S. W. Nixon, *A Coastal Marine Ecosystem, Simulation and Analysis*, 217 pp., Springer-Verlag, New York, 1978.

Large, W. G., and S. Pond, Sensible and latent heat flux measurements over the ocean, *J. Phys. Oceanogr.*, *12*, 464–482, 1982.

Large, W. G., J. C. McWilliams, and S. C. Doney, Oceanic vertical mixing: A review and a model with a nonlocal boundary layer parameterization, *Rev. Geophys.*, *32*, 363–403, 1994.

Levitus, S., Climatological atlas of the world ocean, *NOAA Prof. Pap. 13*, 173 pp., U.S. Govt. Print. Off., Washington, D. C., 1982.

Levitus, S., M. E. Conkright, J. L. Reid, R. G. Najjar, and A. Mantyla, Distribution of nitrate, phosphate and silicate in the world oceans, *Prog. Oceanogr.*, *31*, 245–273, 1993.

Lewis, M. R., J. J. Cullen, and T. Platt, Relationships between vertical mixing and photoadaptation of phytoplankton: Similarity criteria, *Mar. Ecol. Prog. Ser.*, *15*, 141–149, 1984.

Li, W. K. W., Temperature adaptation in phytoplankton: Cellular and photosynthetic characteristics, in *Primary Production in the Sea*, edited by P. G. Falkowski, pp. 259–279, Plenum, New York, 1980.

Li, W. K. W., and I. Morris, Temperature adaptation in *Phaeodactylum tricornutum bohlin*: Photosynthetic rate compensation and capacity, *J. Exp. Mar. Biol. Ecol.*, *58*, 135–150, 1982.

Li, W. K. W., H. J. C. Smith, and T. Platt, Temperature response of photosynthetic capacity and carboxylase activity in Arctic marine phytoplankton, *Mar. Ecol. Prog. Ser.*, *17*, 237–243, 1984.

Lizotte, M. P., and K. R. Arrigo, Parameterization of a spectral model of primary production in the Southern Ocean (abstract), *Eos Trans. AGU*, *75*(3), Ocean Sci. Meet. Suppl., 217, 1994.

Marra, J., and C. Ho, Initiation of the spring bloom in the northeast Atlantic (47°N, 20°W): A numerical simulation, *Deep Sea Res., Part II*, *40*, 55–73, 1993.

Martin, J. H., R. M. Gordon, S. Fitzwater, and W. W. Broenkow, VERTEX: Phytoplankton/iron studies in the Gulf of Alaska, *Deep Sea Res., Part A*, *36*, 649–680, 1989.

Martin, P. J., Simulation of the mixed layer at OWS November and Papa with several models, *J. Geophys. Res.*, *90*, 903–916, 1985.

Mayzaud, P., and S. A. Poulet, The importance of the time factor in the response of zooplankton to varying concentrations of naturally occurring particulate matter, *Limnol. Oceanogr.*, *23*, 1144–1154, 1978.

McAllister, C. D., Estimates of the transfer of primary production at Ocean Station P, in *Biological Oceanography of the Northern Pacific*

Ocean, edited by A. Y. Takenouti, pp. 575–580, Idemitsu Shoten, Tokyo, 1972.

McClain, C. R., and J. K. Firestone, An investigation of Ekman upwelling in the North Atlantic, *J. Geophys. Res.*, *98*, 12,327–12,339, 1993.

Miller, C. B., B. W. Frost, B. Booth, P. A. Wheeler, M. R. Landry, and N. Welschmeyer, Ecological processes in the subarctic Pacific: Iron limitation cannot be the whole story, *Oceanography*, *4*, 71–78, 1991.

Monahan, E. C., and I. O'Muircheartaigh, Optimal power-law description of oceanic whitecap coverage dependence on wind speed, *J. Phys. Oceanogr.*, *10*, 2094–2099, 1980.

Monod, J., *Recherches sur la Croissance des Cultures Bacteriennes*, Hermann, Paris, 1942.

Morel, A., Optical modeling of the upper ocean in relation to its biogenous matter content (case I waters), *J. Geophys. Res.*, *93*, 10,749–10,768, 1988.

Morel, A., and L. Prieur, Analysis of variations in ocean color, *Limnol. Oceanogr.*, *22*, 709–722, 1977.

Mueller, J. L., and R. E. Lang, Bio-optical provinces of the northeast Pacific Ocean: A provisional analysis, *Limnol. Oceanogr.*, *34*, 1572–1586, 1989.

National Oceanographic Data Center, Oceanographic Station Profile Time Series, *Environ. Inf. Bull. 93-3*, Washington, D. C., 1993.

Neuberger, H., *Introduction to Physical Meteorology*, 271 pp., Pa. State Coll., University Park, 1951.

Ocean Studies Board, *The Ocean's Role in Global Change*, 85 pp., Natl. Acad. Press, Washington, D. C., 1994.

Pond, S., and G. L. Pickard, *Introductory Dynamic Oceanography*, 241 pp., Pergamon, Tarrytown, N. Y., 1978.

Press, W. H., B. P. Flannery, S. A. Teukolsky, and W. T. Vetterling, *Numerical Recipes in C, The Art of Scientific Computing*, 735 pp., Cambridge Univ. Press, New York, 1988.

Reinecker, M. M., and L. L. Ehret, Wind stress curl variability over the North Pacific from the Comprehensive Ocean-Atmosphere Data Set, *J. Geophys. Res.*, *93*, 5069–5077, 1988.

Smith, W. L., Note on the relationship between total precipitable water and surface dew point, *J. Appl. Meteorol.*, *5*, 726–727, 1966.

Steeman-Nielsen, E., V. K. Hansen, and E. G. Jorgensen, The adaptation to different light intensities in *Chlorella vulgaris* and the time dependence on transfer to a new intensity, *Physiol. Plant. Suppl.*, *15*, 505–517, 1962.

Subcommittee on Global Change Research, *Our Changing Planet, The FY 1995 U.S. Global Change Research Program*, 132 pp., Off. of Sci. and Technol. Policy, Washington, D. C., 1995.

Tai, K.-S., and C. R. McClain, A PC-based interactive data analysis package for meteorological and oceanographic data, paper presented at Eighth International Conference on Interactive Information and Processing Systems for Meteorology, Oceanography and Hydrology, Am. Meteorol. Soc., Atlanta, Ga., Jan. 5–10, 1992.

Tai, K.-S., and C. R. McClain, Recent enhancements of IDAPAK, a PC-based interactive data analysis package, paper presented at Ninth International Conference on Interactive Information and Processing Systems for Meteorology, Oceanography, and Hydrology, Am. Meteorol. Soc., Anaheim, Calif., Jan. 17–22, 1993.

Tetens, O., Öbereinige meteorologische Begriffe, *Z. Geophys.*, *6*, 297–309, 1930.

Venrick, E. L., Phytoplankton seasonality in the central North Pacific: The endless summer reconsidered, *Limnol. Oceanogr.*, *38*, 1135–1149, 1993.

Venrick, E. L., J. A. McGowan, D. R. Cayan, and T. L. Hayward, Climate and chlorophyll a: Long-term trends in the central North Pacific Ocean, *Science*, *238*, 70–72, 1987.

Welschmeyer, N., R. Goericke, S. Strom, and W. Peterson, Phytoplankton growth and herbivory in the subarctic Pacific: A chemotaxonomic analysis, *Limnol. Oceanogr.*, *36*, 1631–1649, 1991.

Welschmeyer, N., S. Strom, R. Goericke, G. DiTullio, M. Blevin, and W. Peterson, Primary production in the subarctic Pacific Ocean: Project SUPER, *Prog. Oceanogr.*, *32*, 101–135, 1993.

Wong, C. S., F. A. Whitney, K. Iseki, J. S. Page, and J. Zeng, Analysis of trends in primary productivity and chlorophyll a over two decades at Ocean Station P (50°N, 145°W) in the subarctic Northeast Pacific Ocean, *Can. J. Fish. Aquat. Sci.*, *121*, 107–117, 1995.

Woodruff, S. D., R. J. Slutz, R. L. Jenne, and P. M. Steurer, A comprehensive ocean-atmosphere data set, *Bull. Am. Meteorol. Soc.*, *68*(10), 1239–1250, 1987.

Wroblewski, J. S., A model of phytoplankton plume formation during variable Oregon upwelling, *J. Mar. Res.*, *35*, 357–394, 1977.

Wroblewski, J. S., and R. G. Richman, The non-linear response of plankton to wind mixing events—Implications for survival of larval northern anchovy, *J. Plankton Res.*, *9*, 103–123, 1987.

K. Arrigo and C. R. McClain, Oceans and Ice Branch, NASA Goddard Space Flight Center, Code 971.0, Greenbelt, MD 20771. (e-mail: mcclain@calval.gsfc.nasa.gov)

K.-S. Tai, General Sciences Corporation, 6100 Chevy Chase Drive, Laurel, MD 20707.

D. Turk, Department of Oceanography, Dalhousie University, Halifax, Nova Scotia, Canada B3H 4J1.

(Received May 17, 1995; revised September 29, 1995; accepted October 3, 1995.)